VIP Biomimetic Models Very Important Paper

International Edition: DOI: 10.1002/anie.201604412
German Edition: DOI: 10.1002/ange.201604412

Deformylation Reaction by a Nonheme Manganese(III)–Peroxo Complex via Initial Hydrogen-Atom Abstraction

Prasenjit Barman, Pranav Upadhyay, Abayomi S. Faponle, Jitendra Kumar, Sayanta Sekhar Nag, Devesh Kumar, Chivukula V. Sastri,* and Sam P. de Visser**

Abstract: *Metal–peroxo intermediates are key species in the catalytic cycles of nonheme metalloenzymes, but their chemical properties and reactivity patterns are still poorly understood. The synthesis and characterization of a manganese(III)–peroxo complex with a pentadentate bispidine ligand system and its reactivity with aldehydes was studied. Manganese(III)–peroxo can react through hydrogen-atom abstraction reactions instead of the commonly proposed nucleophilic addition reaction. Evidence of the mechanism comes from experiments which identify a primary kinetic isotope effect of 5.4 for the deformylation reaction. Computational modeling supports the established mechanism and identifies the origin of the reactivity preference of hydrogen-atom abstraction over nucleophilic addition.*

The chemistry of metal–dioxygen intermediates has attracted interest in the field of biological as well as bioinorganic chemistry communities for many decades. These complexes are key intermediates in the catalytic cycles of metalloenzymes that activate and utilize molecular oxygen for vital biological processes in the human body, including the metabolism of drugs and the biosynthesis of hormones.[1] Although many metalloenzymes use iron as the central cofactor, several actually use manganese instead. Biologically active manganese ions are included, for instance, in the oxygen-evolving complex of photosystem II,[2] but also in superoxide dismutase that catalyzes the detoxification of superoxide and hydrogen peroxide to water.[3] The manganese–peroxo intermediate has been postulated as an important intermediate in these catalytic cycles; however, as it is short-lived, there currently is no experimental evidence available. Therefore, synthetic biomimetic models have been developed that have a ligand architecture suitable for studies in solution but have a coordination sphere that resembles enzyme analogues and consequently may give insight into the chemical and spectroscopic properties of enzymatic intermediates and their reactivity patterns.[4]

In the past few years, several biomimetic metal–peroxo adducts of iron and manganese have been prepared and characterized with UV/Vis, electronic absorption, electron paramagnetic resonance (EPR), and X-ray absorption spectroscopy techniques.[5,6] Furthermore, reactivity patterns with model substrates were studied, which showed that these metal–peroxo species mainly react through nucleophilic addition reactions.[7,8] Recently, a nonheme manganese(III)–peroxo complex with cyclam-type ligand was spectroscopically characterized with electronic absorption, EPR, and X-ray absorption techniques. Moreover, the complex was shown to react with manganese(II) chloride to form manganese(IV)–oxo and manganese(III)–hydroxo complexes.[9]

Synthetic metal–peroxo complexes are known to react with aldehydes efficiently in a proposed nucleophilic reaction mechanism. However, an alternative mechanism, not considered previously, concerns a rate determining hydrogen-atom abstraction from the α-position prior to oxygen-atom transfer. Recent work on metal–bispidine ligand systems showed that these complexes react efficiently with substrates through hydrogen-atom abstraction, owing to their rigid ligand framework, and reaction rates could be monitored effectively over a broad temperature and concentration range.[10] Therefore, we decided to investigate the relative reactivity of the $[Mn^{III}(L^1)(O_2)]^+$ complex (Scheme 1) with aldehydes and study the possible nucleophilic addition versus hydrogen-atom abstraction mechanisms. In particular, we report the synthesis and characterization of a novel side-on manganese(III)–peroxo complex with a pentadentate bispidine N5 ligand, $[Mn^{III}(L^1)(O_2)]^+$ (**1**),[11] Scheme 1, and study its reactivity patterns with 2-phenylpropionaldehyde (2-PPA) and its α-deuterated form.

The starting manganese(II) complex, $[Mn^{II}(L^1)(ClO_4)_2]^{2+}$ (**2**), was synthesized by reacting $Mn^{II}(ClO_4)_2{\cdot}2CH_3CN$ with the pentadentate bispidine ligand (L^1) in CH_3CN under an argon atmosphere, in analogy to previously reported procedures.[12] Addition of 10 equivalents of H_2O_2 to a colorless solution containing $[Mn^{II}(L^1)(ClO_4)_2]^{2+}$ (**2**; 2 mM) and triethylamine (TEA; 2.5 equivalents) in an acetonitrile solution at 15 °C afforded a blue intermediate (**1**) with an absorption band at 605 nm ($\varepsilon = 270\ L\,mol^{-1}\,cm^{-1}$; with a half-life of about 60 minutes (Figure 1a; see the Supporting Information for experimental details). The blue intermediate is characterized with various spectroscopic techniques including UV/Vis, high-

[*] P. Barman, S. S. Nag, Dr. C. V. Sastri
Department of Chemistry, Indian Institute of Technology Guwahati
Assam, 781039 (India)
E-mail: sastricv@iitg.ernet.in
P. Upadhyay, J. Kumar, Dr. D. Kumar
Department of Applied Physics, School of Physical Sciences
Babasaheb Bhimrao Ambedkar University
Lucknow, 226025 (India)
E-mail: dkclcre@yahoo.com
A. S. Faponle, Dr. S. P. de Visser
Manchester Institute of Biotechnology and School of Chemical Engineering and Analytical Science, The University of Manchester
131 Princess Street, Manchester M1 7DN (UK)
E-mail: sam.devisser@manchester.ac.uk
Supporting information and the ORCID identification number(s) for the author(s) of this article can be found under http://dx.doi.org/10.1002/anie.201604412.

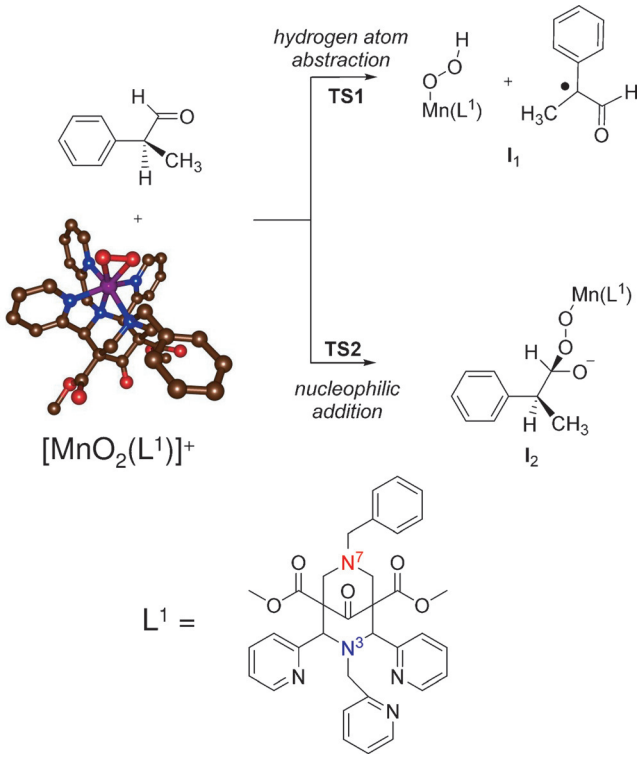

Scheme 1. Reactant complex $[Mn^{III}(L^1)(O_2)]^+$ and the possible reactivity patterns with 2-PPA substrate.

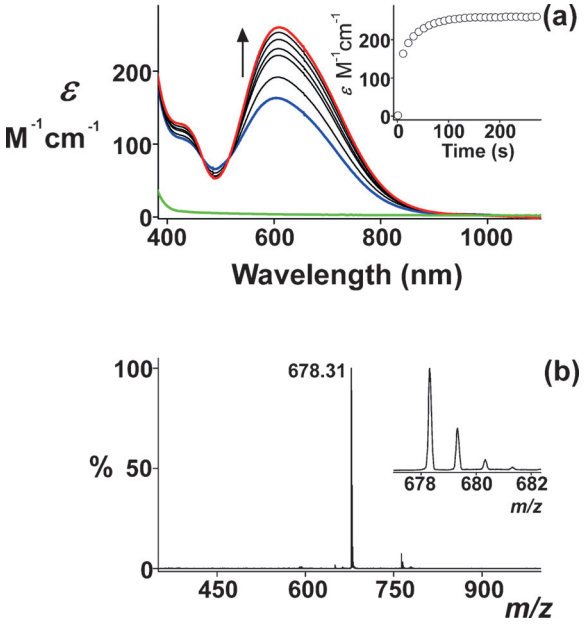

Figure 1. a) UV/Vis spectra of formation of **1** (2 mM) upon addition of $[Mn(L^1)]^{2+}$ (**2**; green line) in the presence of TEA (5 mM) and H_2O_2 (20 mM) in CH_3CN at 15 °C. Inset: the time trace for the formation the **1**. b) ESI-MS spectrum of **1**. Inset: the observed isotope distribution patterns for $[Mn(L^1)(O_2)]^+$.

resolution electrospray ionization-mass spectrometry (ESI-MS), and DFT. The ESI mass spectra of **1** exhibit a prominent ion peak with *m*/*z* 678.31, its isotopic distribution pattern

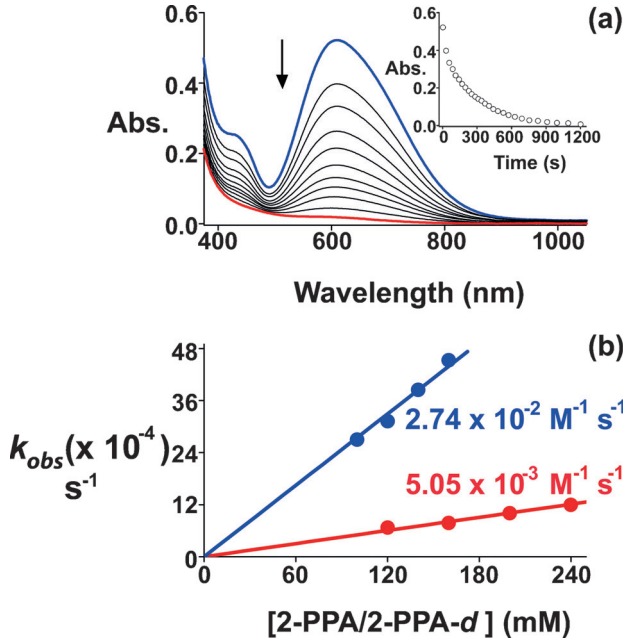

Figure 2. Kinetics of the reaction of **1** with 2-PPA: a) UV/Vis spectral changes of **1** (2 mM) upon addition of 2-PPA (160 mM) in the presence of TEA (5 mM) and hydrogen peroxide (20 mM) in CH_3CN at 15 °C. Inset: time course of the absorbance at 605 nm. b) Plot of k_{obs} against the concentration of 2-PPA and α-[D_1]-PPA (ca. 90%, D-enriched) and the derived second-order rate constant for the reaction of 2 mM **1** with substrate at various concentrations in CH_3CN at 15 °C for 2-PPA (●, blue) and α-[D_1]-PPA (●, red).

corresponds to $[Mn^{III}(L^1)(O_2)]^+$ (Figure 1b). These spectra are similar to those found by Jackson et al. on an analogous manganese(III)–peroxo complex.[9]

The nucleophilic and electrophilic character of **1** was then investigated in a reaction with 2-PPA as a substrate. Previous work showed that manganese(III)–peroxo complexes react with aldehydes to give the corresponding deformylated products by attacking the carbonyl group in a nucleophilic reaction.[6c,d] Upon addition of 2-PPA to **1** in CH_3CN at 15 °C, the intermediate decayed immediately and led to acetophenone as product (Figure 2a). The pseudo first-order rate constant of the decay of **1** increased linearly with increasing 2-PPA concentration, thus giving a second-order rate constant of 2.74×10^{-2} L mol^{-1} s^{-1}.

To establish whether the mechanism proceeds through a nucleophilic attack on the carbonyl group we used 2-methyl-2-phenylpropionaldehyde (2-Me-2-PPA) as a mechanistic probe. Upon addition of 2-Me-2-PPA to **1** at 15 °C, the intermediate decays at the rate of its natural decay. However, when the reaction solutions were analyzed with ESI-MS no deformylated products were observed. These results demonstrate that the manganese(III)–peroxo does not react with 2-PPA through a nucleophilic attack on the carbonyl group. As such, the work contradicts previous studies on the reactivity of nonheme and heme metal–peroxo complexes with aldehydes, that all reported a nucleophilic mechanism.[5b,6a,13]

To find out whether an alternative pathway was possible starting with an initial hydrogen-atom abstraction, we decided to investigate the reaction with α-[D_1]-PPA. Thus, upon

addition of α-[D_1]-PPA (ca. 90%, D-enriched) to **1** in CH_3CN at 15 °C we determined a second-order rate constant of 5.05×10^{-3} L mol^{-1} s^{-1} (Figure 2b). Therefore, our kinetics studies establish the manganese(III)–peroxo complex to react with 2-PPA via a rate determining hydrogen-atom abstraction reaction from the α-position with a kinetic isotope effect (KIE) of 5.4.

To find further evidence of this novel reaction mechanism, we performed a radical trapping experiment with bromotrichloromethane using procedures reported previously.[14] Addition of 2-PPA to intermediate **1** in the presence of excess CCl_3Br (or CBr_4) in CH_3CN at 15 °C, leads to the formation of α-brominated product of the 2-PPA exclusively, which was confirmed by NMR analysis (Supporting Information). Consequently, our kinetics and reactivity studies clearly reveal a novel reaction mechanism between manganese(III)–peroxo complexes with aldehydes starting from an α-hydrogen-atom abstraction step.

To gain further insight into the rate determining step for the reaction of manganese(III)–peroxo with aldehydes, we decided to follow the experimental work up with a set of density functional theory calculations using previously reported procedures.[15] Two pathways were investigated, namely 1) hydrogen-atom abstraction by **1** from the α-position of 2-PPA; and 2) nucleophilic attack of the peroxo group on the carbonyl moiety of 2-PPA. The optimized geometries of the hydrogen-atom abstraction (^{5}**TS**$_{HA}$) and nucleophilic transition state (^{5}**TS**$_{NA}$) are given in the Supporting Information, Figures S15 and S18. Herein, we will focus on the analysis of the results and the understanding as to why the hydrogen-atom abstraction pathway is favorable. The hydrogen-atom abstraction barrier is relatively central with close values of the C–H and H–O distances and as expected happens with a large imaginary frequency for the C–H–O stretch typical for hydrogen-atom abstraction reactions.[16] In agreement with experimental observation the lowest barrier is ^{5}**TS**$_{HA}$ ($\Delta E + ZPE^{\ddagger} = 23.9$ kcal mol^{-1}). By contrast, the nucleophilic transition state (^{5}**TS**$_{NA}$) is well higher in energy ($\Delta E + ZPE^{\ddagger} = 28.7$ kcal mol^{-1}).

To understand the mechanistic preference of hydrogen-atom abstraction over nucleophilic addition, we devised a novel two-parabola curve crossing diagram to explain the reaction mechanism, which shows analogy to the valence bond curve crossing diagrams of Shaik.[17] Figure 3 shows details of the two-parabola curve crossing model. Thus, we consider the reaction along the reaction coordinate (x) that starts in the reactants (at $x = 0$) that is connected to another local minimum at $x = 1$ via a reaction barrier. We assume that the potential energy curve (y) can be described with a parabola with function $y_R = ax^2$ for the reactant complex and $y_P = bx^2 + cx + d$ for the products. If we assume that the transition state for the reaction happens at a reaction coordinate $x = {}^1/_2$ then these two curves will cross at $x = {}^1/_2$ and using the values for $y_P(0)$, $y_P({}^1/_2)$, $y_P(1)$, and $y_P'(1)$, we can derive an equation for the curve crossing energy (ΔE_{cross}) as a function of the Franck-Condon energy in the reactants

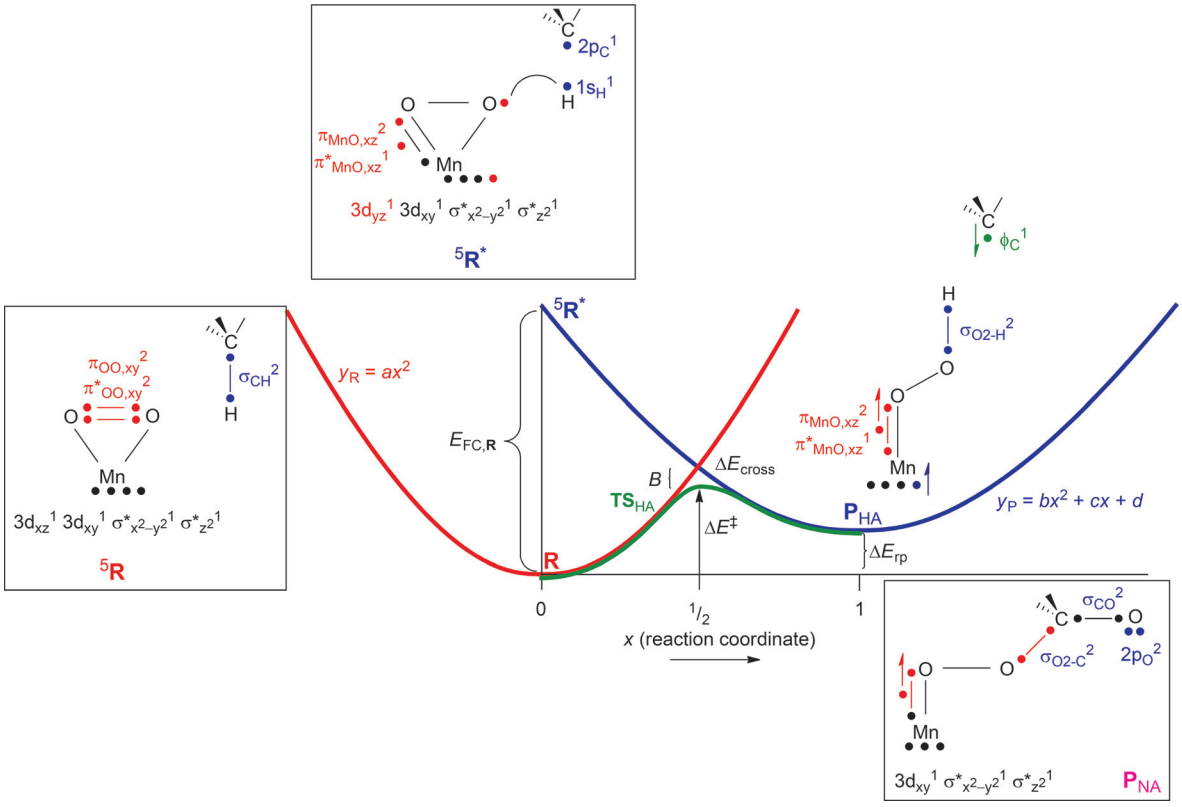

Figure 3. Two-parabola curve-crossing rationalization of the hydrogen-atom abstraction pathway in the reaction of **1** with 2-PPA. Bond orbital changes along the pathways highlighted. Dots represent electrons, and a line between two dots is a bond occupied by two electrons. Straight arrows indicate spin orbitals. Also shown is the VB representation of the alternative nucleophilic intermediate **P**$_{NA}$.

($E_{FC,\mathbf{R}}$) and the driving force for the reaction (ΔE_{rp}), Equation (1), as defined in Figure 3.

$$\Delta E_{cross} = {}^1\!/_4 E_{FC,R} + {}^3\!/_4 \Delta E_{rp} \quad (1)$$

As shown previously using valence-bond curve-crossing diagrams,[17] the actual transition state is below the curve crossing energy by an amount B (the resonance energy), so that we can predict the value of the transition state based on estimates for $E_{FC,\mathbf{R}}$, ΔE_{rp}, and B with Equation (2).

$$\Delta E^{\neq}{}_{VB,HAT} = \Delta E_{cross} - B \quad (2)$$

We then analyzed the bond breaking and orbital changes between reactants, transition states and intermediates for the rate determining reaction step to predict the Franck–Condon energy between $^5\mathbf{R}$ and $^5\mathbf{R}$* and give details in Figure 3 in a valence bond format. These VB schemes were used previously to predict reactivities and rationalize reactivity trends.[18,19] Thus, the hydrogen-atom abstraction is accomplished through the breaking of the σ_{CH} bond of the substrate leading to atomic $2p_C$ and $1s_H$ orbitals, which energetically is equal to the bond dissociation energy of the C–H bond (BDE_{CH}). On the oxidant side of the reaction the $\pi_{OO,xy}{}^2$ $\pi^*{}_{OO,xy}{}^2$ pair of orbitals revert back to atomic orbitals and will cost an energy $E_{O=O}$. This will generate two doubly occupied 2p atomic orbitals, one on each oxygen atom. One of those 2p electrons on the terminal oxygen atom will form a bond with the incoming hydrogen atom, while the other electron is transferred to the $3d_{yz}$ orbital on Mn. Finally, the other 2p orbital on oxygen atom O1 will form a three-electron bond with the $3d_{xz}$ orbital on manganese and form the $\pi_{MnO,xz}$ and $\pi^*{}_{MnO,xz}$ pair of orbitals. The Franck–Condon energy, therefore, can be described as the sum of BDE_{CH}, $E_{O=O}$, and E_{ET}. We calculate a BDE_{CH} value for the α-position of 2-PPA of 80.3 kcal mol^{-1}, while the energy difference between the $\pi_{OO,xy}$ and $\pi^*{}_{OO,xy}$ was found to be 129.1 kcal mol^{-1} in the side-on manganese(III)–peroxo complex. Finally, the excitation energy from $\pi^*{}_{OO,xy}$ to $3d_{yz}$ was estimated to be 96.6 kcal mol^{-1}. The resonance energy, as before,[17] was taken as one half of the weakest bonds that are either broken or formed, which in this case is the sum of the O–H and Mn–O bond. As such, we estimate a hydrogen-atom abstraction barrier of 24.5 kcal mol^{-1}, which is in excellent agreement with the DFT barrier reported above.

Subsequently, we investigated the bond breaking and electron rearrangements for the nucleophilic addition reaction of which we show the VB representation of the product configuration in Figure 3. The reaction is initiated with the breaking of the carbonyl π-bond ($E_{PPA,\pi}$) as well as the splitting of the $\pi_{OO,xy}{}^2$ $\pi^*{}_{OO,xy}{}^2$ pair of orbitals on the peroxo group into atomic orbitals, that is, $E_{O=O}$. Similarly to the hydrogen-atom abstraction process the $2p_{O1}$ pair of electrons form a three-electron bond with the $3d_{xz}$(Mn) electron. Finally, a C–O bond is formed between peroxo and carbonyl. However, in contrast to the hydrogen-atom abstraction process no electron transfer from peroxo to manganese takes place. Instead, two electrons from the peroxo are donated into the C–O bond and the two electrons from the C=O π-bond move to the carbonyl oxygen atom. The resonance energy for the nucleophilic pathway is one-half of the sum of the C–O and Mn–O bonds that are formed, while a value of $E_{PPA,\pi=}$184.7 kcal mol^{-1} was estimated. Based on first principles, we estimate the nucleophilic barrier to be $\Delta E^{\neq}{}_{VB,NA} = 44.9$ kcal mol^{-1}.

The VB modeling, therefore, predicts that the side-on manganese–peroxo will react with 2-PPA through preferential α-hydrogen-atom abstraction rather than via nucleophilic addition. This is possible thanks to its small redox potential that enables efficient electron transfer from peroxo to manganese, which is a lower energy pathway than transferring an electron from peroxo to substrate carbonyl. Furthermore, the C–H bond strength of the substrate is only 80.3 kcal mol^{-1} and despite the fact that the side-on peroxo will give a weaker O–H bond, actually a strong Mn–O three-electron bond is formed, which gives the reaction to large driving force. By contrast, the nucleophilic pathway gains a rather weak C–O bond probably due to stereochemical repulsions of the ligand substituents interfering with the bond formation, so that this process overall will cost more energy. Therefore, the side-on manganese–peroxo with bispidine ligand system will preferentially react via hydrogen-atom abstraction rather than nucleophilic addition with aldehydes through its availability of low-energy metal 3d orbitals that can pick up an electron from the peroxo group. Further research will need to be done on synthetic and enzymatic manganese and iron–peroxo complexes, such as the aldehyde deformylating dioxygenases,[20] to find out whether this is a general mechanism.

Acknowledgements

Research support was provided by the Department of Science and Technology (SERB), India (EMR/2014/000279) to C.V.S. The National Service of Computational Chemistry Software (NSCCS) is acknowledged for CPU time to S.d.V. A.S.F. thanks the Tertiary Education Trust Fund Nigeria for a studentship. D.K. is the Ramanujan Fellow of the Department of Science and Technology, New Delhi (India).

Keywords: biomimetic models · density functional theory · enzyme models · hydrogen-atom abstraction · reaction mechanisms

How to cite: *Angew. Chem. Int. Ed.* **2016**, *55*, 11091–11095
Angew. Chem. **2016**, *128*, 11257–11261

[1] a) *Biomimetic Oxidations Catalyzed by Transition Metal Complexes* (Ed.: B. Meunier), Imperial College Press, London, **2000**; b) *Cytochrome P450: Structure, Mechanism, and Biochemistry*, 3rd ed. (Ed.: P. R. Ortiz de Montellano), Kluwer Academic/Plenum Publishers, New York, **2005**.

[2] a) D. J. Vinyard, G. M. Ananyev, G. C. Dismukes, *Annu. Rev. Biochem.* **2013**, *82*, 577–606; b) G. Renger, T. Renger, *Photosynth. Res.* **2008**, *98*, 53–80; c) J. Barber, *Q. Rev. Biophys.* **2003**, *36*, 71–89; d) P. E. M. Siegbahn, *Chem. Eur. J.* **2008**, *14*, 8290–8302.

[3] a) T. A. Jackson, T. C. Brunold, *Acc. Chem. Res.* **2004**, *37*, 461–470; b) B. R. Streit, B. Blanc, G. S. Lukat-Rodgers, K. R. Lukat-Rodgers, J. L. Dubois, *J. Am. Chem. Soc.* **2010**, *132*, 5711–5724;

c) S. Hofbauer, C. Gruber, K. F. Pirker, A. Sündermann, I. Schaffner, C. Jakopitsch, C. Oostenbrink, P. G. Furtmüller, C. Obinger, *Biochemistry* **2014**, *53*, 3145 – 3157.
[4] a) M. Costas, M. P. Mehn, M. P. Jensen, L. Que, Jr., *Chem. Rev.* **2004**, *104*, 939 – 986; b) P. C. A. Bruijnincx, G. van Koten, R. J. M. Klein Gebbink, *Chem. Soc. Rev.* **2008**, *37*, 2716 – 2744; c) M. M. Abu-Omar, A. Loaiza, N. Hontzeas, *Chem. Rev.* **2005**, *105*, 2227 – 2252; d) S. V. Kryatov, E. V. Rybak-Akimova, S. Schindler, *Chem. Rev.* **2005**, *105*, 2175 – 2226.
[5] a) G. Roelfes, V. Vrajmasu, K. Chen, R. Y. N. Ho, J.-U. Rohde, C. Zondervan, R. M. la Crois, E. P. Schudde, M. Lutz, A. L. Spek, R. Hage, B. L. Feringa, E. Münck, L. Que, Jr., *Inorg. Chem.* **2003**, *42*, 2639 – 2653; b) J. Annaraj, Y. Suh, M. S. Seo, S. O. Kim, W. Nam, *Chem. Commun.* **2005**, 4529 – 4531; c) A. Thibon, J.-F. Bartoli, S. Bourcier, F. Banse, *Dalton Trans.* **2009**, 9587 – 9594; d) A. Mukherjee, M. A. Cranswick, M. Chakrabarti, T. K. Paine, K. Fujisawa, E. Münck, L. Que, Jr., *Inorg. Chem.* **2010**, *49*, 3618 – 3628; e) J. Cho, S. Jeon, S. A. Wilson, L. V. Liu, E. A. Kang, J. J. Braymer, M. H. Lim, B. Hedman, K. O. Hodgson, J. S. Valentine, E. I. Solomon, W. Nam, *Nature* **2011**, *478*, 502 – 505.
[6] a) J. Annaraj, J. Cho, Y.-M. Lee, S. Y. Kim, R. Latifi, S. P. de Visser, W. Nam, *Angew. Chem. Int. Ed.* **2009**, *48*, 4150 – 4153; *Angew. Chem.* **2009**, *121*, 4214 – 4217; b) D. F. Leto, S. Chattopadhyaay, V. W. Day, T. A. Jackson, *Dalton Trans.* **2013**, *42*, 13014 – 13025; c) M. Zlatar, M. Gruden, O. Y. Vassilyeva, E. A. Buvaylo, A. N. Ponomarev, S. A. Zvyagin, J. Wosnitza, J. Krzystek, P. Garcia-Fernandez, C. Duboc, *Inorg. Chem.* **2016**, *55*, 1192 – 1201; d) C.-M. Lee, C.-H. Chuo, C.-H. Chen, C.-C. Hu, M.-H. Chiang, Y.-J. Tseng, C.-H. Hu, G.-H. Lee, *Angew. Chem. Int. Ed.* **2012**, *51*, 5427 – 5430; *Angew. Chem.* **2012**, *124*, 5523 – 5526.
[7] W. Nam, *Acc. Chem. Res.* **2007**, *40*, 522 – 531.
[8] a) M. K. Coggins, J. A. Kovacs, *J. Am. Chem. Soc.* **2011**, *133*, 12470 – 12473; b) M. K. Coggins, V. Martin-Diaconescu, S. DeBeer, J. A. Kovacs, *J. Am. Chem. Soc.* **2013**, *135*, 4260 – 4272.
[9] H. E. Colmer, A. W. Howcroft, T. A. Jackson, *Inorg. Chem.* **2016**, *55*, 2055 – 2069.
[10] a) P. Comba, M. Kerscher, W. Schiek, *Prog. Inorg. Chem.* **2007**, *55*, 613 – 704; b) P. Comba, S. Fukuzumi, H. Kotani, S. Wunderlich, *Angew. Chem. Int. Ed.* **2010**, *49*, 2622 – 2625; *Angew. Chem.* **2010**, *122*, 2679 – 2682.
[11] L^1 = dimethyl-2,4-di(2-pyridyl)3-(pyridin-2-ylmethyl)-7-benzyl-3,7-diaza-bicyclo[3.3.1] nonan-9-one-1,5-dicarboxylate.
[12] P. Barman, A. K. Vardhaman, B. Martin, S. J. Wörner, C. V. Sastri, P. Comba, *Angew. Chem. Int. Ed.* **2015**, *54*, 2095 – 2099; *Angew. Chem.* **2015**, *127*, 2123 – 2127.
[13] a) M. S. Seo, J. Y. Kim, J. Annaraj, Y. Kim, Y.-M. Lee, S.-J. Kim, J. Kim, W. Nam, *Angew. Chem. Int. Ed.* **2007**, *46*, 377 – 380; *Angew. Chem.* **2007**, *119*, 381 – 384; b) R. A. Geiger, S. Chattopadhyay, V. W. Day, T. A. Jackson, *Dalton Trans.* **2011**, *40*, 1707 – 1715; c) Y. Goto, S. Wada, I. Morishima, Y. Watanabe, *J. Inorg. Biochem.* **1998**, *69*, 241 – 247; d) J. Cho, R. Sarangi, J. Annaraj, S. Y. Kim, M. Kubo, T. Ogura, E. I. Solomon, W. Nam, *Nat. Chem.* **2009**, *1*, 568 – 572; e) R. L. Shook, W. A. Gunderson, J. Greaves, J. W. Ziller, M. P. Hendrich, A. S. Borovik, *J. Am. Chem. Soc.* **2008**, *130*, 8888 – 8889; f) J. Cho, R. Sarangi, H. Y. Kang, J. Y. Lee, M. Kubo, T. Ogura, E. I. Solomon, W. Nam, *J. Am. Chem. Soc.* **2010**, *132*, 16977 – 16986; g) R. V. Ottenbacher, D. G. Samsonenko, E. P. Talsi, K. P. Bryliakov, *ACS Catal.* **2016**, *6*, 979 – 988; h) J. A. Kovacs, *Acc. Chem. Res.* **2015**, *48*, 2744 – 2753; i) C.-M. Lee, C.-H. Chuo, C.-H. Chen, C.-C. Hu, M.-H. Chiang, Y.-J. Tseng, C.-H. Hu, G.-H. Lee, *Angew. Chem. Int. Ed.* **2012**, *51*, 5427 – 5430; *Angew. Chem.* **2012**, *124*, 5523 – 5526.
[14] a) J. T. Groves, T. E. Nemo, *J. Am. Chem. Soc.* **1983**, *105*, 6243 – 6248; b) S. Rana, A. Dey, D. Maiti, *Chem. Commun.* **2015**, *51*, 14469 – 14472.
[15] a) A. K. Vardhaman, P. Barman, S. Kumar, C. V. Sastri, D. Kumar, S. P. de Visser, *Angew. Chem. Int. Ed.* **2013**, *52*, 12288 – 12292; *Angew. Chem.* **2013**, *125*, 12514 – 12518; b) S. P. de Visser, M. G. Quesne, B. Martin, P. Comba, U. Ryde, *Chem. Commun.* **2014**, *50*, 262 – 282; c) S. Kumar, A. S. Faponle, P. Barman, A. K. Vardhaman, C. V. Sastri, D. Kumar, S. P. de Visser, *J. Am. Chem. Soc.* **2014**, *136*, 17102 – 17115.
[16] L. Ji, A. S. Faponle, M. G. Quesne, M. A. Sainna, J. Zhang, A. Franke, D. Kumar, R. van Eldik, W. Liu, S. P. de Visser, *Chem. Eur. J.* **2015**, *21*, 9083 – 9092.
[17] a) S. S. Shaik, *J. Am. Chem. Soc.* **1981**, *103*, 3692 – 3701; b) S. Shaik, *Phys. Chem. Chem. Phys.* **2010**, *12*, 8706 – 8720.
[18] a) D. Kumar, B. Karamzadeh, G. N. Sastry, S. P. de Visser, *J. Am. Chem. Soc.* **2010**, *132*, 7656 – 7667; b) D. Kumar, R. Latifi, S. Kumar, E. V. Rybak-Akimova, M. A. Sainna, S. P. de Visser, *Inorg. Chem.* **2013**, *52*, 7968 – 7979.
[19] A. S. Faponle, M. G. Quesne, S. P. de Visser, *Chem. Eur. J.* **2016**, *22*, 5478 – 5483.
[20] L. J. Rajakovich, H. Nørgard, D. M. Warui, W.-C. Chang, N. Li, S. J. Booker, C. Krebs, J. M. Bollinger, Jr., M.-E. Pandelia, *J. Am. Chem. Soc.* **2015**, *137*, 11695 – 11709.

Received: May 6, 2016
Revised: June 3, 2016
Published online: July 8, 2016

